

Ortho-Positronium Three-Photon Decays: Physics Constraints and a Closed-Form Energy Method for Annihilation Vertex Reconstruction

L. Raczyński*, W. Krzemień†, A. Coussat‡
M. Bała, B.C. Hiesmayr§
K. Klimaszewski, M. Obara, R. Y. Shopa

April 2026

Abstract

We examine the physical foundations of ortho-positronium three-photon decay in the context of annihilation vertex reconstruction, focusing on how energy–momentum conservation constrains the space of physically admissible solutions. Finally, we provide a closed-form analytical derivation of an energy-based vertex reconstruction algorithm.

1 Introduction

Positronium is one of the simplest purely leptonic bound states known in nature, consisting of an electron and a positron (the antimatter partner of the electron) held together by their mutual Coulomb attraction. The solution of the Schrödinger equation describing this quasi-atom is the same as for the hydrogen atom, except that Bohr’s radius is four times greater. Positronium decays via annihilation of the constituent positron either with its bound electron or with electrons from the surrounding medium. It exists in two spin configurations: para-positronium (p-Ps), with a lifetime in vacuum of 124 ps, which predominantly decays into two photons, and ortho-positronium (o-Ps), which decays

*L. Raczyński, M. Bała, K. Klimaszewski, M. Obara, R. Y. Shopa are with the National Centre for Nuclear Research, Department of Complex Systems, 05-400 Otwock, Poland (e-mail: lech.raczynski@ncbj.gov.pl).

†W. Krzemień is with the National Centre for Nuclear Research, Department of High Energy Physics, 05-400 Otwock, Poland (e-mail: wojciech.krzemien@ncbj.gov.pl).

‡A. Coussat is with INSA-Lyon, Université Claude Bernard Lyon 1, CNRS, Inserm, CREATIS UMR 5220, U1294, F-69373, Lyon, France (e-mail: aurelien.coussat@creatis.insa-lyon.fr).

§B. C. Hiesmayr is with the IT:U Interdisciplinary Transformation University, Freistädter Strasse 400, 4040 Linz, and University of Vienna, Faculty of Physics, Währingerstrasse 17, 1090 Vienna, Austria.

mainly into three photons and has a mean lifetime in vacuum of 142 ns [1]. Positronium and its properties have been the subject of various fundamental studies, including precision tests of quantum electrodynamics (QED) [2], measurements of discrete symmetry violations [3–5], investigations of correlations in photon polarization degrees of freedom [6–15] and positronium’s wave nature [16].

Since annihilation photons carry information about both the positronium system itself and the microscopic environment in which it annihilates, positronium serves as a sensitive probe of biological and material environments. For instance, positronium (Ps) is used in material science and engineering studies, where the PALS technique provides direct information about defect structures in materials [17]. Recently, the positronium-based marker has been discussed and studied in the context of positron emission tomography (PET) medical imaging [18]. In the conventional PET imaging, the functional image of the patient is obtained by reconstructing the spatial distribution of the radiotracer concentration from photon pairs produced by annihilation of positrons emitted by an administered radiotracer. By measuring properties of the positronium system, which precedes annihilation in biological tissues in approximately 40% of cases [19], additional diagnostically relevant information about the local environment can be extracted.

The proposed markers include: (i) the positronium lifetime [20–27], which is shortened by interactions with the surrounding medium through pick-off annihilation [28, 29] and spin-exchange processes [30, 31], and (ii) the ratio of number of three to two photon decays. The latter has been studied as a diagnostic observable sensitive to microstructure [32], and has also found use in materials science for the characterisation of porous media and gas diffusion [33, 34]. A broader overview of positronium applications in biology and medicine is provided in [18].

Two main classes of three-photon vertex reconstruction methods have been proposed. The first and earliest relies on energy-momentum conservation to derive the vertex position from the measured photon energies [32, 35, 36]. Initial feasibility was demonstrated through simulations and proof-of-principle measurements with HP-Ge and NaI(Tl) detectors. More recently, a similar approach was used to produce the first three-to-two ratio image of point sources with GAGG scintillator detectors and ^{18}F -FDG, achieving a spatial resolution of approximately 1.1 cm without tomographic reconstruction or time-of-flight (TOF) information [37]. The energy-based approach requires energy resolutions of a few per cent, which are not achieved by current clinical PET systems. The second class employs a time-based trilateration strategy which reconstructs the vertex from photon arrival times and interaction positions alone [38]. While relaxing the energy resolution requirement, this approach currently achieves a spatial resolution of approximately 8 cm [39].

The remainder of this article is organised as follows. Section 2 derives the physical constraints imposed by energy-momentum conservation on candidate vertex positions, establishes the triangle condition, and discusses both uninformative and QED-informed prior distributions over the decay vertex. Section 3

presents the closed-form analytical solution of the energy-based vertex reconstruction algorithm.

2 Physical constraints on the three-photon decay and prior distribution over the annihilation vertex

Let us consider the decay of o-Ps at rest into three photons described by the momenta $\vec{\omega}_1, \vec{\omega}_2, \vec{\omega}_3$. The energy of the annihilation photons may be written as $E_i = \hbar\omega_i$ for $i \in \{1, 2, 3\}$ with $\omega_i = |\vec{\omega}_i|$ and without loss of generality \hbar is set to 1. Therefore, the momentum-energy conservation equations are:

$$\vec{\omega}_1 + \vec{\omega}_2 + \vec{\omega}_3 = \vec{0} \quad (1)$$

$$\omega_1 + \omega_2 + \omega_3 = 2m_e c^2 \quad (2)$$

as the total energy of the o-Ps at rest is equal to the sum of masses of its constituent e^- and e^+ , equivalent to twice the mass of the electron, where we neglect the binding energy of a few eV. Subsequently, all derivations are given in the o-Ps rest frame.

Equation (1) implies that any momentum vector lies in the plane spanned by the remaining two, so all three vectors are coplanar. Since photon tracks are straight lines from the decay point \mathbf{x} , the decay point itself lies in the same plane. Assuming the hit positions \vec{P}_i for $i \in \{1, 2, 3\}$ are measured with high precision, they define the decay plane and reduce the reconstruction problem to a 2-D space.

Let us comment on the assumption that we consider o-Ps to be at rest, and therefore we know its total energy beforehand. In practice, this assumption is well justified, e.g. in tissues since the probability of Ps formation depends on the positron kinetic energy and it is strongly peaked near smaller values below 50 eV [40].

2.1 Triangle condition on the decay vertex

Momentum conservation imposes a further geometric constraint on the candidate vertex \mathbf{x} within the decay plane. Defining the unit vectors from \mathbf{x} toward each hit as

$$\vec{n}_i(\mathbf{x}) = \frac{\vec{P}_i - \mathbf{x}}{|\vec{P}_i - \mathbf{x}|}, \quad (3)$$

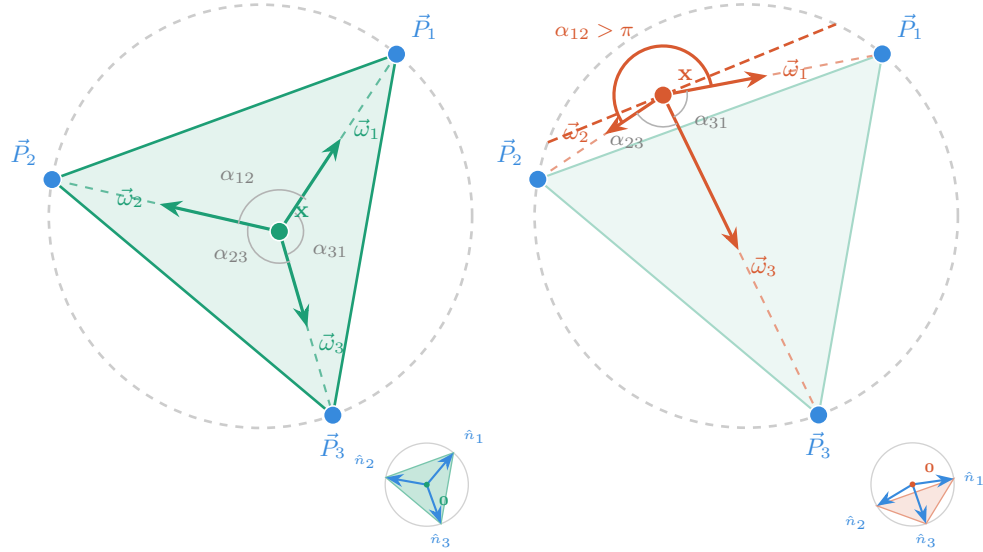
and writing $\vec{\omega}_i = \omega_i \vec{n}_i(\mathbf{x})$ for massless photons, Eq. (1) becomes:

$$\sum_{i=1}^3 \omega_i \vec{n}_i(\mathbf{x}) = \vec{0}, \quad \omega_i > 0. \quad (4)$$

A solution with all $\omega_i > 0$ exists if and only if the directions $\vec{n}_i(\mathbf{x})$ surround \mathbf{x} , i.e., no straight line through \mathbf{x} places all three hits on the same side. Equivalently, the largest opening angle between consecutive directions as seen from \mathbf{x} must satisfy:

$$\max_{i \neq j} \alpha_{ij}(\mathbf{x}) < \pi. \quad (5)$$

The set of all \mathbf{x} satisfying (5) is exactly the interior of the triangle $\triangle \vec{P}_1 \vec{P}_2 \vec{P}_3$. Outside, all directions \vec{n}_i lie within an open half-plane and their positive linear combination cannot vanish (see Figs. 1a and 1b).



(a) Valid vertex ($\max \alpha_{ij} < \pi$): $\mathbf{x} \in \triangle \vec{P}_1 \vec{P}_2 \vec{P}_3$. Unit vectors surround \mathbf{x} ; their weighted sum can vanish, satisfying momentum conservation with all $\omega_i > 0$.

(b) Invalid vertex ($\max \alpha_{ij} > \pi$): $\mathbf{x} \notin \triangle \vec{P}_1 \vec{P}_2 \vec{P}_3$. All unit vectors lie within an open half-plane (separated by the dashed line); no positive linear combination can vanish.

Figure 1: Triangle condition for candidate vertex \mathbf{x} : a physical solution to momentum conservation requires \mathbf{x} to lie strictly inside $\triangle \vec{P}_1 \vec{P}_2 \vec{P}_3$.

2.2 Role of energy conservation and detector measurements

Energy conservation (2) adds one scalar equation to the geometric constraints. Its practical effect depends on which quantities are measured, and it is instructive to consider two cases.

(i) **No detector energy measurements.** For each candidate \mathbf{x} inside the triangle, momentum conservation already fixes the ratios $\omega_1 : \omega_2 : \omega_3$ from

geometry consideration alone. Since the Ps mass $M = 2m_e c^2$ is known a priori, it fixes the overall energy scale, making a definite prediction $\tilde{\omega}_i(\mathbf{x})$ for each photon energy at each \mathbf{x} . Every interior point remains geometrically reachable, but it converts each candidate vertex into a testable energy prediction.

(ii) Energy measurements available. When the detector measures photon energies E_i , these must be consistent with the predicted values $\tilde{\omega}_i(\mathbf{x})$. With perfect measurements, this selects a unique point \mathbf{x}^* inside the triangle. Under finite detector energy resolution σ_E , the constraint broadens into a likelihood.

Let us note that the energy measurement constrains the directions $\vec{n}_i(\mathbf{x})$ and thereby the ratios of photon momenta. In contrast, the TOF measurements constrain the distances $|\vec{P}_i - \mathbf{x}|$, placing \mathbf{x} on circles centred on each detector hit. The two measurement types are therefore geometrically complementary.

2.3 Prior distribution

Since the hit positions \vec{P}_i are treated as precisely known for our reconstruction, all consequences of energy-momentum conservation are fully determined before any energy or timing measurement is made. They therefore constitute prior knowledge about the candidate vertex \mathbf{x} , independent of the detector responses. Coplanarity, the triangle condition, and the QED-based decay dynamics can, therefore, be treated as a part of the prior.

The first constraint is of a geometrical nature: a physical solution requires \mathbf{x} to lie inside $\triangle \vec{P}_1 \vec{P}_2 \vec{P}_3$, as established in (5). This defines the support of the prior.

The second constraint comes from the QED decay dynamics: given a candidate \mathbf{x} , the predicted energies $\tilde{\omega}_i(\mathbf{x})$ are fixed by geometry via the sine rule (see Section 3), and their probability is given by the Ore–Powell matrix element [1, 41]:

$$P(\tilde{\omega}_1, \tilde{\omega}_2) \propto \sum_{i=1}^3 \left(\frac{m_e c^2 - \tilde{\omega}_i}{\tilde{\omega}_j \tilde{\omega}_k} \right)^2, \quad \{i, j, k\} = \{1, 2, 3\} \quad (6)$$

Equation (6), illustrated in Fig. 2, modulates the prior within its support:

$$P(\mathbf{x}) = \kappa \sum_{i=1}^3 \left(\frac{m_e c^2 - \tilde{\omega}_i(\mathbf{x})}{\tilde{\omega}_j(\mathbf{x}) \tilde{\omega}_k(\mathbf{x})} \right)^2 \cdot \mathbf{1}_{\mathbf{x} \in \triangle \vec{P}_1 \vec{P}_2 \vec{P}_3}, \quad i, j, k \in \{1, 2, 3\}, \quad (7)$$

where κ is a normalisation constant. The indicator function $\mathbf{1}_{\mathbf{x} \in \triangle}$ enforces the hard geometric boundary, while the Ore–Powell factor assigns a higher probability to vertex positions corresponding to kinematically favoured energy configurations, independently of the measured times and energies. Replacing the Ore–Powell factor by a constant recovers the flat Dalitz baseline [42], representing genuine ignorance about the energy sharing among the three photons.

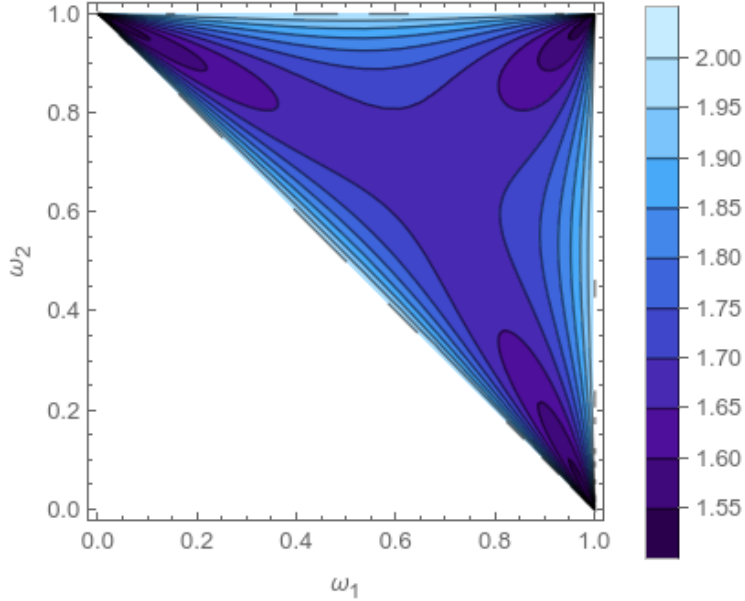


Figure 2: The unnormalized probability distribution $P(\tilde{\omega}_1, \tilde{\omega}_2)$ over the kinematically accessible phase space, shown as a function of normalised photon energies $\tilde{\omega}_i/m_e c^2 \in (0, 1)$.

3 Energy-based position reconstruction derivation

In the following, we present a derivation of the exact solution of the energy-based o-Ps position reconstruction. The vector sum of ω_i elements expresses the momentum conservation law (see Eq. 1), and may be represented by a triangle with angles $\theta_{12} + \theta_{13} + \theta_{23} = \pi$ calculated using the cosine rule:

$$(2m_e c^2 - \omega_i - \omega_j)^2 = \omega_i^2 + \omega_j^2 - 2\omega_i\omega_j \cos \theta_{ij}, \quad 1 \leq i < j \leq 3. \quad (8)$$

The dependence between the angles in the triangle defined by the momentum vectors (θ_{ij}) and the opening angles (α_{ij}) is given by:

$$\theta_{ij} + \alpha_{ij} = \pi \quad 1 \leq i < j \leq 3. \quad (9)$$

and it is illustrated in Fig. 3.

We analyze data in a shifted and rotated decay plane (x'', y''). The points P_1 , P_2 and P_3 corresponding to the coordinates of the three registered hits are situated on the decay plane (x'', y'') as shown in Fig. 4. The origin of the (x'', y'') plane is attached to the P_1 point that is the vertex of the triangle P_1, P_2, P_3

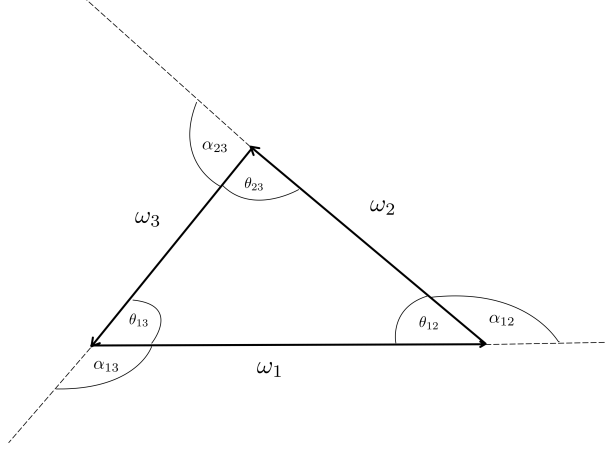


Figure 3: Relation between angles in the triangle defined by the momentum vectors (θ_{ij}) and the opening angles (α_{ij}).

lying at the smallest angle γ_{23} :

$$\gamma_{23} = \min(\gamma_{12}, \gamma_{13}). \quad (10)$$

Under the assumption that the decay point is on the y'' -axis with a negative ordinate value (see Fig. 4), the rotation angle of the triangle (γ) is in the second quadrant. Taking into account additionally Eq. (10), the limits of γ are:

$$\frac{2\pi}{3} \leq \gamma \leq \pi.$$

The rotation angle of the triangle (γ) as well as the distances between the points P_i and decay position (r_i) for $i \in \{1, 2, 3\}$ are unknown. This derivation will be focused only on the estimation of the r_1 distance that is used to parameterize the lines

$$y'' = a_2 x'' - r_1 \quad (11)$$

$$y'' = a_3 x'' - r_1 \quad (12)$$

passing through the decay position and points P_2 and P_3 , respectively. The slopes of the lines a_2 and a_3 can be calculated based on opening angles α_{12} and α_{13} , respectively as:

$$a_2 = \tan\left(\frac{\pi}{2} - \alpha_{12}\right) \quad (13)$$

$$a_3 = \tan\left(\frac{\pi}{2} + \alpha_{13}\right), \quad (14)$$

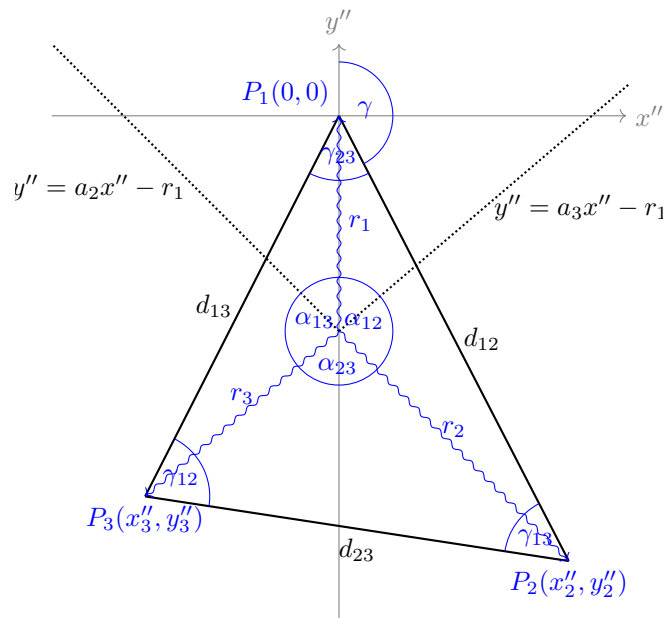


Figure 4: Reconstruction of decay position using energy (equivalently angle) constraints.

where the periodicity of π of the tangent function was taken into account. It is evident that the points P_2 and P_3 in polar representation depend only on the single unknown γ , describing the rotation of the triangle, i.e.

$$\begin{aligned} x_2'' &= d_{12} \sin \gamma & x_3'' &= d_{13} \sin(\gamma + \gamma_{23}) \\ y_2'' &= d_{12} \cos \gamma & y_3'' &= d_{13} \cos(\gamma + \gamma_{23}). \end{aligned} \quad (15)$$

Subtracting the line equation in Eq. (12) for (x_3'', y_3'') from the line equation in Eq. (11) for (x_2'', y_2'') defines the linear dependence of the cartesian coordinates (x_2'', y_2'') and (x_3'', y_3'') :

$$a_2 x_2'' - y_2'' = a_3 x_3'' - y_3''. \quad (16)$$

After substitution of polar coordinates from Eqs. (15) and (16) it is possible to evaluate the rotation angle γ :

$$\gamma = \pi + \arctan \left(\frac{d_{12} + d_{13} (a_3 \sin \gamma_{23} - \cos \gamma_{23})}{a_2 d_{12} - d_{13} (a_3 \cos \gamma_{23} + \sin \gamma_{23})} \right). \quad (17)$$

The additional shift of π is due to the value of the arctan function in the range from $-\frac{\pi}{2}$ to $\frac{\pi}{2}$; as mentioned γ is in the second quadrant (see Fig. 4). Next, the distances r_1 , r_2 and r_3 may be evaluated using sine rule:

$$\begin{aligned} r_1 &= d_{12} \frac{\sin(\gamma - \alpha_{12})}{\sin \alpha_{12}} \\ r_2 &= d_{12} \frac{\sin(\pi - \gamma)}{\sin \alpha_{12}} \\ r_3 &= d_{13} \frac{\sin(\gamma + \gamma_{23} - \pi)}{\sin \alpha_{13}}. \end{aligned}$$

With the distances r_1, r_2, r_3 at hand, the o-Ps position (\mathbf{x}_E) may be found in the original decay plane (x, y) , as a solution of the non-linear system of equations:

$$(x_E - x_i)^2 + (y_E - y_i)^2 = r_i^2, \quad i \in \{1, 2, 3\} \quad (18)$$

describing three circles O_i each with radii r_i for $i \in \{1, 2, 3\}$. The unique solution (x_E, y_E) may be obtained directly by solving the linear system of equations

$$\mathbf{H} \begin{pmatrix} x_E \\ y_E \end{pmatrix} = \mathbf{r} \quad (19)$$

where

$$\mathbf{H} = 2 \begin{pmatrix} x_1 - x_2 & y_1 - y_2 \\ x_1 - x_3 & y_1 - y_3 \end{pmatrix} \quad (20)$$

and

$$\mathbf{r} = \begin{pmatrix} r_2^2 - r_1^2 + x_1^2 - x_2^2 + y_1^2 - y_2^2 \\ r_3^2 - r_1^2 + x_1^2 - x_3^2 + y_1^2 - y_3^2 \end{pmatrix} \quad (21)$$

evaluated based on Eq. (18) by subtracting the circle equation O_j from circle equation O_i for $i < j$.

4 Conclusion

We have analysed the physical constraints imposed by energy-momentum conservation and the QED-based matrix element on the three-photon decay of ortho-positronium and discussed their implications for annihilation vertex reconstruction.

Momentum conservation alone establishes two nested geometrical constraints: coplanarity reduces the reconstruction problem from three to two dimensions, and the triangle condition confines all physically admissible candidate vertices to the interior of the triangle formed by the three photon hit positions. These constraints are determined entirely by the measured hit positions and are independent of any energy or timing measurement.

Energy conservation, combined with the known positronium mass, converts each candidate vertex inside the triangle into a unique, testable prediction for the three photon energies via the sine rule (see Section 3). When detector energy measurements are available, this prediction selects a unique true vertex under perfect resolution. TOF measurements provide geometrically complementary information, constraining distances rather than directions.

The QED decay dynamics, described by the Ore-Powell matrix element, modulate the prior within the triangular support. The resulting distribution, shown in Fig. 2, enhances the probability of configurations in which one photon is soft (carries little energy), corresponding to the edges of the Dalitz plot where $\omega_i \rightarrow 0$.

Finally, we have presented a closed-form analytical derivation of the energy-based vertex reconstruction algorithm. The algorithm exploits the angular constraints imposed by momentum conservation to reduce the problem to a linear system, yielding a unique solution for the annihilation vertex in the decay plane without requiring iterative optimisation.

References

- [1] A. Ore and J. L. Powell. “Three-Photon Annihilation of an Electron-Positron Pair”. In: *Physical Review* 75.11 (June 1949), pp. 1696–1699.
- [2] G. Adkins et al. “Precision Spectroscopy of Positronium: Testing Bound-State QED Theory and the Search for Physics beyond the Standard Model”. In: *Physics Reports* 975 (Sept. 2022), pp. 1–61.
- [3] P. A. Vetter and S. J. Freedman. “Search for *CPT*-Odd Decays of Positronium”. In: *Phys. Rev. Lett.* 91 (26 Dec. 2003), p. 263401.
- [4] T. Yamazaki et al. “Search for *CP* Violation in Positronium Decay”. In: *Phys. Rev. Lett.* 104 (8 Feb. 2010), p. 083401.
- [5] M. S. Allen et al. “Measurement of Positronium Decays at 7T with NeuroSphere PET Modules”. In: *2025 IEEE Nuclear Science Symposium (NSS), Medical Imaging Conference (MIC) and Room Temperature Semiconductor Detector Conference (RTSD)*. Yokohama, Japan: IEEE, Nov. 2025.

- [6] B. C. Hiesmayr and P. Moskal. “Genuine Multipartite Entanglement in the 3-Photon Decay of Positronium”. In: *Sci Rep* 7.1 (Nov. 2017), p. 15349.
- [7] P. Moskal et al. “Feasibility Studies of the Polarization of Photons beyond the Optical Wavelength Regime with the J-PET Detector”. In: *Eur. Phys. J. C* 78.11 (Nov. 2018), p. 970.
- [8] B. C. Hiesmayr et al. “Quantum Error Channels in High Energetic Photonic Systems”. In: *Sci Rep* 14.1 (Apr. 2024), p. 9672.
- [9] S. Parashari et al. “Closing the Door on the “Puzzle of Decoherence” of Annihilation Quanta”. In: *Physics Letters B* 852 (May 2024), p. 138628.
- [10] P. Caradonna. “Kinematic Analysis of Multiple Compton Scattering in Quantum-Entangled Two-Photon Systems”. In: *Annals of Physics* 470 (Nov. 2024), p. 169779.
- [11] P. Caradonna et al. “Stokes-Parameter Representation for Compton Scattering of Entangled and Classically Correlated Two-Photon Systems”. In: *Phys. Rev. A* 109.3 (Mar. 2024), p. 033719.
- [12] J. Bordes et al. “First Detailed Study of the Quantum Decoherence of Entangled Gamma Photons”. In: *Phys. Rev. Lett.* 133.13 (Sept. 2024), p. 132502.
- [13] M. Bała et al. “Probing Arbitrary Polarized Photon Pairs Undergoing Double Compton Scatterings by a Dedicated MC Simulator Validated with Experimental Data”. In: *Eur. Phys. J. C* 85.10 (Oct. 2025), p. 1115.
- [14] P. Žugec et al. “A Reconciliation of the Pryce-Ward and Klein-Nishina Statistics for Semi-Classical Simulations of Annihilation Photons Correlations”. In: *Physics Letters B* 875 (Apr. 2026), p. 140346.
- [15] A. M. Kožuljević et al. “Towards Polarization-Enhanced PET: Study of Random Background in Polarization-Correlated Compton Events”. In: *Physica Medica* 145 (May 2026), p. 105780.
- [16] Y. Nagata et al. “Observation of Positronium Diffraction”. In: *Nat Commun* 17.1 (Dec. 2025), p. 1159.
- [17] Y. Jean et al. *Principles and applications of positron & positronium chemistry*. World Scientific, 2003.
- [18] A. Hourlier et al. “Experimental Uses of Positronium and Potential for Biological Applications”. In: *IEEE Transactions on Radiation and Plasma Medical Sciences* 8.6 (July 2024), pp. 581–594.
- [19] M. D. Harpen. “Positronium: Review of Symmetry, Conserved Quantities and Decay for the Radiological Physicist”. In: *Medical Physics* 31.1 (Dec. 2003), pp. 57–61.
- [20] P. Moskal et al. “Positronium Image of the Human Brain in Vivo”. In: *Science Advances* 10.37 (Sept. 2024), eadp2840.
- [21] R. Y. Shopa and K. Dulski. “Positronium imaging in J-PET with an iterative activity reconstruction and a multistage fitting algorithm”. In: *Bio-Algorithms and Med-Systems* 19.1 (2023), pp. 54–63.

- [22] W. M. Steinberger et al. “Positronium Lifetime Validation Measurements Using a Long-Axial Field-of-View Positron Emission Tomography Scanner”. In: *EJNMMI Physics* 11.1 (Aug. 2024), p. 76.
- [23] B. Huang et al. “Fast High-Resolution Lifetime Image Reconstruction for Positron Lifetime Tomography”. In: *Communications Physics* 8.1 (2025), p. 181.
- [24] L. Mercolli et al. “First positronium lifetime imaging with scandium-44 on a long axial field-of-view PET/CT”. In: *Frontiers in Nuclear Medicine* 5 (2025).
- [25] L. Mercolli et al. “Phantom Imaging Demonstration of Positronium Lifetime with a Long Axial Field-of-View PET/CT and ^{124}I ”. In: *EJNMMI Physics* 12.1 (Aug. 2025), p. 80.
- [26] S. Takyu et al. “Positronium Lifetime Measurement Using a Clinical PET System for Tumor Hypoxia Identification”. In: *Nuclear Instruments and Methods in Physics Research Section A: Accelerators, Spectrometers, Detectors and Associated Equipment* 1065 (Aug. 2024), p. 169514.
- [27] B. Huang et al. “High-Resolution Positronium Lifetime Tomography at Clinical Activity Levels on the PennPET Explorer”. In: *Journal of Nuclear Medicine* 66.9 (Sept. 2025), pp. 1464–1470.
- [28] W. Brandt et al. “Positronium Decay in Molecular Substances”. In: *Physical Review* 120.4 (Nov. 1960), pp. 1289–1295.
- [29] N. T. Trung et al. “Investigation of Ortho-Positronium Annihilation for Porous Materials with Different Geometries and Topologies”. In: *Scientific Reports* 13.1 (Aug. 2023), p. 13707.
- [30] B. Zgardzińska et al. “Ortho-para spin conversion of Ps by paramagnetic O₂ dissolved in organic compounds”. In: *Nukleonika* 60.4 (2015), pp. 801–804.
- [31] P. S. Stepanov et al. “Interaction of Positronium with Dissolved Oxygen in Liquids”. In: *Physical Chemistry Chemical Physics* 22.9 (2020), pp. 5123–5131.
- [32] K. Kacperski et al. “Three-Gamma Annihilation Imaging in Positron Emission Tomography”. In: *IEEE Transactions on Medical Imaging* 23.4 (Apr. 2004), pp. 525–529.
- [33] S. C. Peovovar et al. “Ratio of Positron Annihilation into Three Photons versus Two”. In: *physica status solidi c* 4.10 (2007), pp. 3447–3450.
- [34] W. E. Kauppila et al. “Investigations of Positronium Formation and Destruction Using $3\text{-}\gamma/2\text{-}\gamma$ Annihilation-Ratio Measurements”. In: *Physical Review Letters* 93.11 (Sept. 2004), p. 113401.
- [35] K. Kacperski and N. M. Spyrou. “Performance of Three-Photon PET Imaging: Monte Carlo Simulations”. In: *Physics in Medicine and Biology* 50.23 (Dec. 2005), pp. 5679–5695.

- [36] E. Abuelhia et al. “Three-Photon Annihilation in PET: 2D Imaging Experiments”. In: *Journal of Radioanalytical and Nuclear Chemistry* 271.2 (Feb. 2007), pp. 489–495.
- [37] M. Fujimoto et al. *Advancing PET through Direct Imaging of Three-Photon Decay Using Pure Positron Emitters*. Dec. 2025.
- [38] A. Gajos et al. “Trilateration-based reconstruction of ortho-positronium decays into three photons with the J-PET detector”. In: *Nuclear Instruments and Methods in Physics Research Section A: Accelerators, Spectrometers, Detectors and Associated Equipment* 819 (2016), pp. 54–59.
- [39] P. Moskal et al. “Testing CPT Symmetry in Ortho-Positronium Decays with Positronium Annihilation Tomography”. In: *Nature Communications* 12.1 (Sept. 2021).
- [40] C. Champion. “Moving from Organ Dose to Microdosimetry: Contribution of the Monte Carlo Simulations”. In: *Braz. arch. biol. technol.* 48.spe2 (Oct. 2005), pp. 191–199.
- [41] V. B. Beresteckij et al. *Quantum Electrodynamics*. 2. ed., reprint. Course of Theoretical Physics / L. D. Landau and E. M. Lifshitz 4. Oxford: Butterworth-Heinemann, 2008.
- [42] R. Dalitz. “CXII. On the Analysis of τ -Meson Data and the Nature of the τ -Meson”. In: *The London, Edinburgh, and Dublin Philosophical Magazine and Journal of Science* 44.357 (Oct. 1953), pp. 1068–1080.